# Understanding and Predicting Profile Structure and Parametric Scaling of Intrinsic Rotation

W. X. Wang[1], B. Grierson[1], S. Ethier[1], J. Chen[1], E. Startsev[1], P. H. Diamond[2], Z. X. Lu[2]
[1]Princeton Plasma Physics Laboratory, P. O. Box 451, Princeton, New Jersey 08543, USA
[2]University of California, San Diego, California, USA

wwang@pppl.gov

**Abstract.** This paper reports on new understanding of intrinsic rotation physics in magnetic fusion through advanced gyrokinetic simulations and the development of a first-principles-based model for predicting intrinsic rotation profile in experiments. It is shown for the first time that turbulent fluctuation-driven residual stress can account for both the shape and magnitude of the observed intrinsic toroidal rotation profile. Specifically, nonlinear, global gyrokinetic simulations of DIII-D ECH plasmas indicate a substantial ITG fluctuation-induced non-diffusive momentum flux generated around a mid-radius-peaked intrinsic toroidal rotation profile. The non-diffusive momentum flux is dominated by the residual stress with a negligible contribution from the momentum pinch. The residual stress profile shows a robust anti-gradient, dipole structure in a set of ECH discharges with varying ECH power. Such interesting features of non-diffusive momentum fluxes, in connection with edge momentum sources and sinks, are found to be critical to drive the non-monotonic core rotation profiles in the experiments. Both turbulence intensity gradient and zonal flow $\mathbf{E}\times\mathbf{B}$ shear are identified as major contributors to the generation of the $k_\parallel$-asymmetry needed for the residual stress generation. By balancing the residual stress and the momentum diffusion, a self-organized, steady-state rotation profile is calculated. The predicted core rotation profiles agree well with the experimental measurements. The radial structure of residual stress profile and associated intrinsic rotation gradient are shown to have a complicated dependence on multiple physics parameters including turbulence type, q-profile structure, and collisionality, through which possible rotation profile optimization can be developed. Interesting results obtained include intrinsic rotation reversal induced by ITG-TEM transition in flat-q profile regime and by change in q-profile from weak to normal shear.

## I. Introduction

Plasma flows, in particular, toroidal rotation can play an important role in controlling plasma macro-stability and improving confinement performance. Toroidal rotation is often driven externally through neutral beam injection in current fusion experiments. However, in future large size devices, the beam torque is expected to be small. Therefore, ITER, for example, may have to rely on plasma self-generated intrinsic rotation for controlling plasma stability and microturbulence.

It is generally believed that there are two key elements for intrinsic rotation generation. The first one is edge momentum sources and sinks which can be due to, for example, particle losses or transport imbalance between trapped and passing particles coupling with edge geometry effects. The second key element is momentum transport, which can bring the edge momentum, either positive or negative, into the core region and form a global rotation profile. In particular, a non-diffusive momentum flux which connects edge momentum sources/sinks and core plasma flow is critical. Plasma turbulence provides a key mechanism for driving toroidal momentum transport. Toroidal angular momentum flux due to turbulence consists of three components as expressed below,

$$\Gamma_\phi \propto -\chi_\phi \frac{\partial U_\phi}{\partial r} + V_p U_\phi + \Pi^{\rm rs}_{r,\phi},$$

e.g., the usual momentum diffusion (first term), and two non-diffusive momentum fluxes which are momentum pinch (second term) and residual toroidal Reynolds stress (third term). The three

components in the momentum flux have different physics origins under turbulence circumstances, and have distinct effects on global profile formation.

After more than a decade of intensive experimental, theoretical and computational studies leading to significant progress in understanding the intrinsic rotation phenomenon, now the fusion community has been asking if we have enough knowledge and valid modeling capability for intrinsic prediction. This paper presents an effort to address this issue. With regard to intrinsic rotation prediction, both its achievable amplitude and profile structure are important since each one may result in different effects on macro- and micro-instabilities.

## II. Outstanding features of turbulence-driven momentum transport in ECH plasmas

Understanding and predicting intrinsic rotation profile structure presents a great challenge and opportunity to test the physics of turbulence-driven intrinsic rotation and validate first-principles-based models. In this paper, we focus on ECH-heated plasmas for our study. A set of DIII-D ECH discharges with different ECH input power are simulated using global nonlinear gyrokinetic simulations. Figure 1 shows how plasma profiles of density, electron temperature, ion temperature and toroidal rotation change as the ECH power increases. The intrinsic rotations observed in those discharges are essentially the plasma self-generated intrinsic rotation because the momentum torque associated with ECH injection is negligible. We use those ECH discharges for this study for several reasons. First, ECH discharges are quite relevant to ITER since ECH power directly goes to electrons and ITER plasmas are expected to be dominated by electron heating. Second, intrinsic rotations observed in those ECH plasmas show very interesting features in global profile structures. Namely, they are non-monotonic with an off-axis peak in the core region. Such off-axis peaked, non-monotonic profiles cannot be generated through pure momentum diffusion process and it is a clear indication of the importance of non-diffusive momentum transport. One unique feature of those DIII-D experiments is that the measurement of toroidal rotation is directly inferred from the main ions rather than merely from impurities as in most previous experiments. Finally, these well-diagnosed DIII-D discharges provide a large amount of experimental data with high quality, which is critical for the purpose of validation.

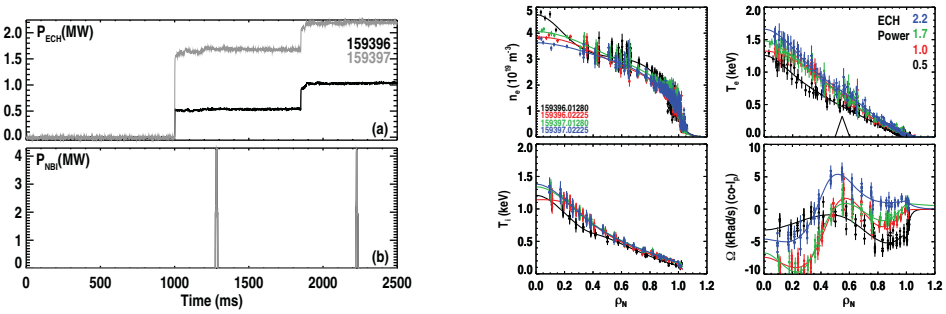


Figure 1: Time history of ECH power and short neutral beam pulses (for main ion rotation measurement) (left) and radial profiles of $n_e$, $T_e$, $T_i$ and ion toroidal rotation (right) from the DIII-D ECH power scan experiments.

The global gyrokinetic simulations carried out with the GTS code [1, 2] for this study take into account the comprehensive influence of many physics effects, including fully kinetic electrons, realistic geometry constructed directly using experimental data, real electron and ion collisions, toroidal flow, and equilibrium electric field. All the plasma profiles and the equilibrium radial electric are directly read from experimental data. Global simulations cover a wide region of minor radii, from $r/a = 0.05$ to 0.9. A large number of simulation particles (60 - 100 particles per cell per species) is used in order to achieve good statistics. Spatial grid size in the perpendicular direction is approximately equal to the local $\rho_i$ (ion gyroradius). In order to separate the three components of the toroidal momentum flux, three independent nonlinear simulations are performed for each cases, using zero toroidal rotation, a rigid toroidal rotation, and the realistic

toroidal rotation, respectively. Correspondingly, the simulated toroidal momentum fluxes in the three simulations are, by definition, purely residual Reynolds stress, both residual stress and momentum pinch, and all three components.

The simulation results show that significant turbulent fluctuations, which are mainly driven by ion temperature gradient (ITG) instabilities, are present in the core region of those DIII-D ECH discharges from 0.4 to 0.8 in minor radius. Turbulence intensity peaks at around $r/a = 0.56$, close to the location of the rotation profile peak. The turbulence is dominated by fluctuations with $k_\theta \rho_s \sim 0.1 - 0.3$, and correspondingly, dominated by toroidal mode numbers from 20 to 60.

The ITG turbulence in those ECH plasmas is found to drive a significant anomalous thermal transport of experimental level. It is also found to drive a substantial residual stress in the core region (see Fig.2). The amplitude of the residual stress can be comparable to that of momentum diffusion.

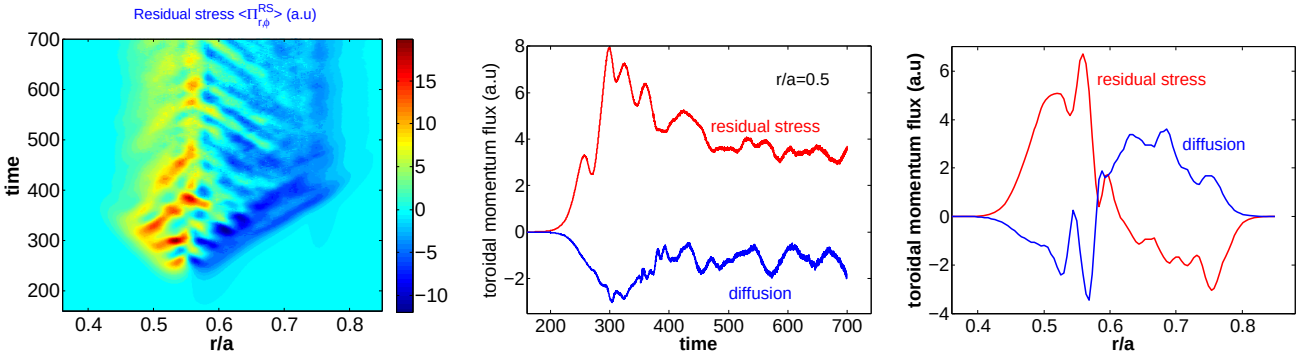


Figure 2: Spatio-temporal evolution of simulated residual stress (left), time history of residual stress and diffusive momentum flux at $r/a = 0.5$ (middle), and radial profile of residual stress and momentum diffusion at steady state (right) due to ITG turbulence in a DIII-D ECH plasma.

Before further discussion of the physics results, it is interesting to examine the property of toroidal momentum conservation [3] in our gyrokinetic simulations. Figure 3 plots the rate of toroidal momentum change and the divergence of residual stress (namely, fluctuation-driven intrinsic torque) during a phase of turbulence development corresponding to the two terms in the following local momentum conservation equation,

$$\frac{\partial}{\partial t}(m_i n_i < RV_\phi >) + < \nabla \cdot \Pi^{RS}_{r,\phi} >= 0,$$

respectively. The two curves are on the top of each other, indicating that the local momentum conservation is well satisfied.

One outstanding feature of turbulence-driven residual stress found here is that it shows an anti-gradient, dipole structure, as illustrated in the right panel of Fig. 2. The residual stress switches sign at $r/a \sim 0.6$. On the other hand, the simulated turbulence-driven momentum diffusion is shown to follow the gradient, as it should be, and the momentum pinch due to turbulence is found to be small. The anti-gradient, dipole structure in the residual stress is found to be critical for the formation of off-axis-peaked core rotation profile. As shown in the right of Fig. 2, the momentum flux associated with the residual stress is outward in the inner core region and inward in the outer core region, which provides a counter-balance against the momentum

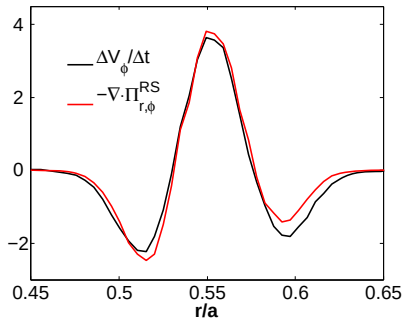


Figure 3: Radial profile of toroidal momentum change rate and intrinsic torque density due to residual stress.

diffusion. This is exactly what is needed to hold a steady state off-axis-peaked core rotation profile.

We now discuss the mechanisms driving the residual stress. A major contribution to the residual stress is parallel Reynolds stress, which needs a finite $k_\parallel$ to be nonvanishing [4]. For most drift-wave instabilities, the modes with positive and negative $k_\parallel$ are equally excited in ideal situations. Namely, there is a perfect reflection symmetry in the $k_\parallel$ spectrum, and a zero $k_\parallel$ on average. Therefore, a critical factor for turbulence to drive residual stress is the presence of physics effects which can break $k_\parallel$-symmetry. Physics mechanisms that may cause such symmetry breaking, and thus the generation of residual Reynolds stress, include finite shear in the $\mathbf{E}\times\mathbf{B}$ velocity [5, 6], turbulence self-generated low frequency zonal flow shear [7], up/down asymmetry in equilibrium geometry[8], radial gradient in the turbulence intensity[9], poloidal tilt of global mode structure arising from the profile shearing [10], and magnetic shear effects on turbulence spectrum [11]. Higher order terms in the gyrokinetic equation are also being investigated as possible drivers for breaking structural symmetry of gyrokinetics in local limit[12].

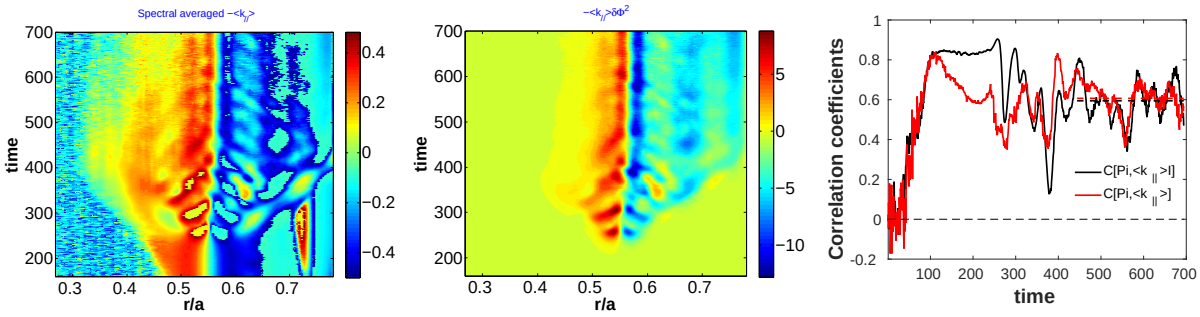


Figure 4: Spatio-temporal evolution of spectral averaged $\langle k_\parallel\rangle$ (left), parallel Reynolds stress based on quasi-linear estimate (middle), and correlation coefficients of simulated toroidal residual stress with $\langle k_\parallel\rangle$ and the parallel Reynolds stress (right).

The global GTS simulations used for this study take into account the global turbulence effects (and the effect of up-down geometric asymmetry) needed for symmetry breaking and turbulence-driven toroidal momentum flux. Such global effects have proven to be significant for turbulence to drive residual stress in many previous gyrokinetic studies. The left panel of Fig. 4 displays the spatio-temporal evolution of spectrum-averaged $k_\parallel$ defined as

$$\langle k_\parallel\rangle(r) \equiv \frac{1}{qR_0}\frac{\sum(n/|n|)(nq-m)\delta\Phi^2_{mn}}{\sum\delta\Phi^2_{mn}},$$

which clearly shows the generation of significant finite $k_\parallel$ due to symmetry breaking in saturated turbulence. The radial profile of the averaged $k_\parallel$ shows a dipole structure which is consistent with the dipole structure observed in the directly calculated residual toroidal Reynolds stress (see Fig. 2). A parallel Reynolds stress estimated by quasi-linear theory shows a similar spatio-temporal structure as the directly simulated residual stress (the middle of Fig. 4). Further quantitative analysis indeed shows strong corrections of the toroidal residual stress with the spectrum-average $k_\parallel$ and the parallel Reynolds stress (the right of Fig. 4).

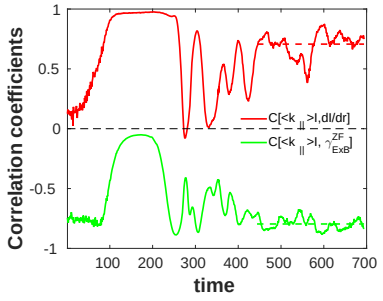


Figure 5: Time history of correlation coefficients of spectral averaged $\langle k_\parallel\rangle(r)$ with turbulence intensity gradient and zonal flow shearing rate.

Further investigation is carried out to identify the cause of $k_\parallel$-symmetry breaking needed for generating residual stress among the various mechanisms previously mentioned. It is found that the spectrum-averaged $k_\parallel$ has strong correlation with both the turbulence self-generated zonal flow shearing rate and turbulence intensity gradient, as shown in Fig. 5. This result suggests

that both turbulence intensity gradient and zonal flow $\mathbf{E}\times\mathbf{B}$ shear are major contributors to the $k_\parallel$-symmetry breaking needed for residual stress generation. On the other hand, the equilibrium $\mathbf{E}\times\mathbf{B}$ shear is shown to be less significant.

**III. First-principles-based model and intrinsic rotation prediction**

We have shown that a significant residual stress is generated by ITG turbulence in these ECH plasmas. But how does residual stress affect the formation of global rotation profile? We now discuss a first-principles-based model for intrinsic rotation prediction, which will also help clarify this question. We start from the toroidal momentum transport equation in the absence of external torque (and the torque of neoclassical toroidal viscosity due to the breaking of toroidal symmetry in magnetic geometry):

$$\frac{\partial}{\partial t}(m_i n_i < RV_\phi >) + < \nabla\cdot\mathbf{\Gamma}_\phi >= 0, \text{ where } \mathbf{\Gamma}_\phi \equiv \int d^3v m_i R v_\phi \mathbf{v}_E \delta f_i.$$

The steady state condition (also taking into account boundary conditions) requires

$$< \mathbf{\Gamma}_\phi\cdot\nabla\rho > \propto -\chi_\phi\frac{\partial U_\phi}{\partial r} + V_p U_\phi + \Pi^{\rm rs}_{r,\phi} = 0.$$

This result states that at the steady state, plasma will self-organize to form a global intrinsic rotation profile so as to make the total momentum flux vanishing everywhere radially. We show below that the turbulence-produced momentum pinch is small (negligible). Thus, the equation reduces to the balance between momentum diffusion and residual stress:

$$m_i n_i \chi_\phi(\rho)\langle R^2|\nabla\rho|\rangle\frac{d\omega_\phi}{d\rho} = \Pi^{\rm rs}_{r,\phi}.$$

This is a one-dimensional ordinary differential equation for determining the intrinsic rotation profile when the residual stress $\Pi^{\rm rs}_{r,\phi}$, momentum diffusivity $\chi_\phi$ and a boundary condition are given. The first-principles-based global gyrokinetic simulation provides the residual stress in the RHS. The momentum diffusivity $\chi_\phi$, in principle, is unknown since in order to calculate $\chi_\phi$ using gyrokinetic simulations we need to know the toroidal rotation which, however, is what we want to predict. Moreover, in the presence of a region of flat toroidal rotation, $\chi_\phi$ can not be determined. Instead, we use the well-known relation, $\chi_\phi(\rho) = P_r\chi_i(\rho)$ to relate the $\chi_\phi$ with the thermal diffusivity $\chi_i$, which can be obtained by our gyrokinetic simulations without knowing the toroidal rotation. Here, $P_r$ is the intrinsic Prandtl number, which is well established both theoretically and experimentally, with a value close to or less than unity [13]. With regard to the boundary condition needed for solving the equation, we directly use experimentally measured toroidal rotation velocity $\omega_\phi$ at the edge region, which is determined by edge physics (which is not covered by the current simulations).

As previously mentioned, the momentum pinch due to turbulence is found to be small. This result is illustrated in Fig. 6 for the ITG case of the ECH plasma (left) and a case of collisionless trapped electron mode (CTEM) turbulence (middle). The red curves are the residual stress profiles obtained from the ITG and CTEM simulations with zero toroidal rotation, and the black curves are the sum of residual stress and momentum pinch, which are obtained from the simulations with a uniform toroidal rotation. For both ITG and CTEM cases, the two curves are almost on the top of each other, indicating that the momentum pinch is small compared to the residual stress. This justifies the neglect of momentum pinch in our model.

We have to use a Prandtl number in our predictive model rather than directly calculating $\chi_\phi$, which is not available. The range of Prandtl number associated with turbulence has been extensively studied both theoretically and experimentally. We should stress that the choice of Prandtl number in our predictive model is not arbitrary but based on our simulation results.

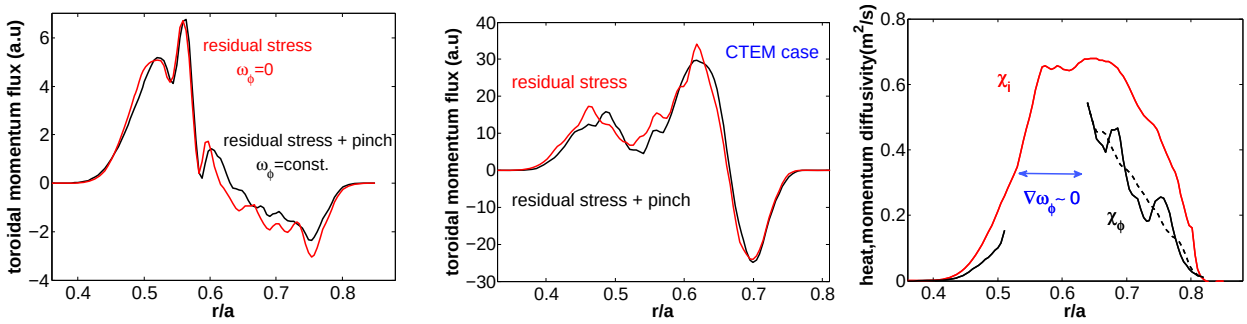


Figure 6: Radial profiles of simulated residual stress and the sum of both residual stress and momentum pinch due to ITG (left) and CTEM (middle) turbulence, and radial profile of simulated ion heat and momentum diffusivity for the DIII-D ECH plasma (right), indicating a Prandtl number $P_r \approx 0.7$ (note that $\chi_\phi$ can not be determined in the region of $\nabla\omega_\phi \sim 0$).

The right panel of Fig. 6 shows the simulated $\chi_i$ and $\chi_\phi$ for the DIII-D ECH discharge. We can see $\chi_\phi$ is slightly smaller than unity in regions of finite rotation gradient where it is well defined. According to this result, we chose $P_r = 0.7$, which is also consistent with previous studies [14].

Now we have all the elements in the model for calculating intrinsic rotation profiles. The result for the ECH discharge of 1.0 MW heating power is presented in Fig. 7, which shows quantitatively good agreement between the predicted intrinsic rotation and experimentally measured main ion toroidal rotation. Moreover, good agreement is obtained for a set of discharges with varying ECH power. In Fig. 7, predictions are made for both using up-down symmetry and up-down asymmetry MHD equilibrium in order to examine the effect of up-down asymmetry in the geometry, which was also proposed as a mechanism for $k_\parallel$-symmetry breaking needed for residual stress generation. The result suggests that the effect of up-down asymmetry in the equilibrium is insignificant. It is worthy to point out that the predicted core rotation profile is not sensitive to the variation in the Prandtl number in the range observed in our gyrokinetic simulations. Quantitative agreement obtained between the first-principles-based prediction and experimental measurements at this level of intrinsic rotation is quite non-trivial and meaningful. To a certain extend, it provides a test and verification for the physics mechanism of turbulence-driven intrinsic rotation, key mechanisms for $k_\parallel$-symmetry breaking for turbulence to generate residual stress, and global gyrokinetic simulation model for calculating momentum transport.

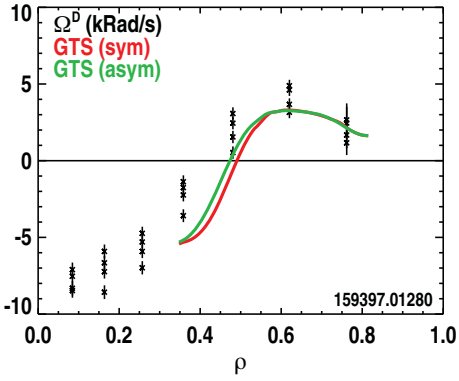


Figure 7: Radial profile of predicted intrinsic rotation in comparison with experimentally measured main ion toroidal rotation in a DIII-D ECH plasma. Red and green lines are predicted intrinsic rotations based on GTS simulations using up-down symmetry and asymmetry equilibrium, respectively.

## IV. Characteristic dependence of intrinsic rotation profile structure

Rotation amplitude and profile structure (e.g., rotation gradient) have different effects on MHD stability and microturbulence. One important question to ask is what determines the radial structure of residual stress and associated intrinsic rotation profile. Through the radial force balance relation, $E_r = \frac{1}{ne}\frac{\partial p}{\partial r} + \frac{1}{c}(B_\theta V_t - B_t V_\theta)$, both pressure gradient and toroidal rotation contribute to $E_r$. In terms of $\mathbf{E}\times\mathbf{B}$ flow generation, it is then very interesting to know whether intrinsic rotation works against or in line with the pressure gradient in contributing to the mean $\mathbf{E}\times\mathbf{B}$ shearing rate. Therefore, understanding the characteristic dependence of residual stress profile structure will help us develop a possible approach for flow control and

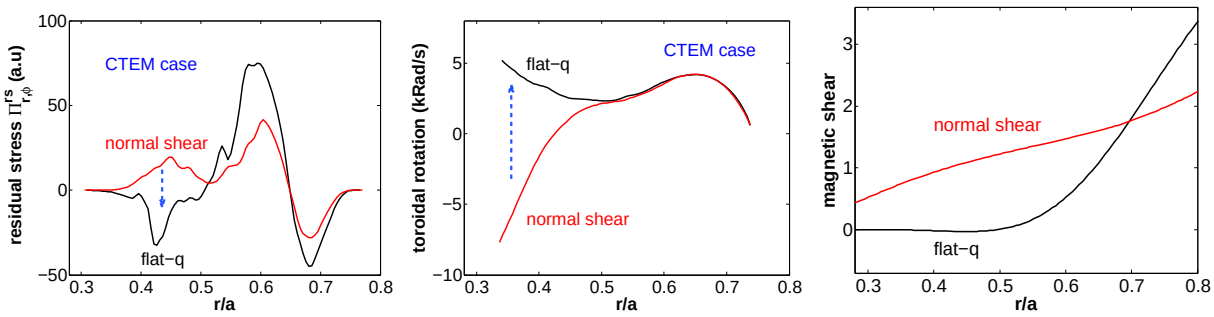


Figure 8: Radial profile of CTEM turbulence driven residual stress (left), intrinsic rotation (middle) from two simulations using different q-profile in equilibria, and magnetic shear of the two equilibria (right).

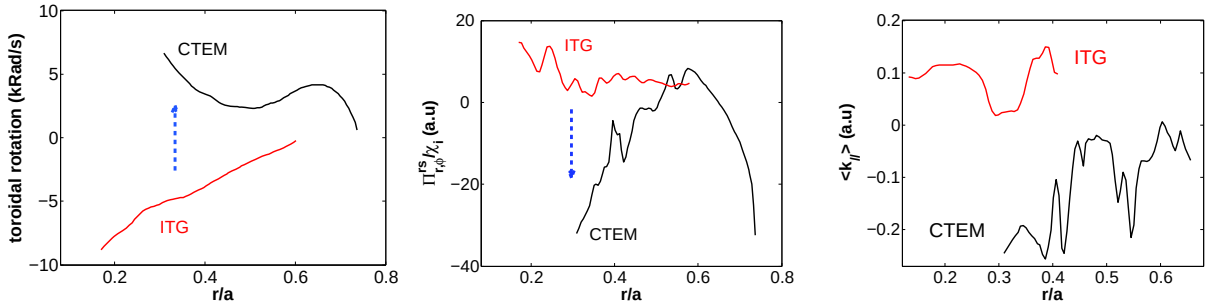


Figure 9: Radial profile of fluctuation driven intrinsic rotations (left), ratio of residual stress and thermal diffusivity (middle) and spectral averaged $\langle k_{\|} \rangle$ (right) due to ITG and CTEM turbulence with a flat-q profile in equilibrium.

optimization. In particular, understanding the intrinsic rotation reversal phenomenon, which has been widely observed in various experiments, is of great interest [15]. One general remark is that the radial structure of residual stress and intrinsic rotation seem to show complicated dependence on multiple physics parameters including turbulence type (for example, ITG vs TEM), q-profile structure (magnetic shear, q-value), collisionality, etc.

Here we use the predictive model described above to examine the magnetic shear effect on intrinsic rotation reversal. Figure 8 presents results of two simulations of CTEM turbulence using different equilibrium with the key difference in q-profile. More specifically, one equilibrium has normal shear while the other has a weak, close to zero, shear in the inner core region. Pressure profile and boundary surface used for generating the two equilibria are the same. The CTEM-driven residual stress is shown to bifurcate in the inner core region as q-profile changes from normal to weak (or zero) shear. Correspondingly, the CTEM-driven intrinsic rotation reverses in the region. The underlying physics is linked to magnetic shear effects on the turbulence spectrum, which provides a new mechanism for the symmetry breaking in low magnetic shear regime by causing a significant radial shift of poloidal mode harmonics [11]. As a result, it introduces a critical value of magnetic shear for the reversal of residual stress orientation and consequently, the reversal of intrinsic rotation. The critical magnetic shear for intrinsic rotation reversal is found to be $\sim 0.3$ in the CTEM regime [16]. It is also noted from Fig. 8 that the intrinsic rotations generated in the two cases are almost the same in the outer core region while the amplitude of CTEM-driven residual stress is significantly lower in the weak shear case. This result highlights the fact that the ratio of $\Pi^{\rm rs}_{r,\phi}/\chi_\phi$, rather than the magnitude of residual stress itself, is critical for determining the intrinsic rotation. Based on this, one may anticipate that any effects of fluctuations that influence ion thermal flux and residual stress in a different way can strongly impact intrinsic rotation profile formation.

The change of underlying turbulence, e.g., from ITG to TEM, is also considered as a possible mechanism responsible for the intrinsic rotation reversal observed in experiments. This is mostly

based on quasilinear arguments and the properties of linear modes. More specifically, the intrinsic rotation reversal is linked to the fact that i) the poloidal tilt of global mode structure switches orientation; and ii) the mode propagation changes from ion to electron diamagnetic direction as turbulence changes from ITG and TEM. Our nonlinear, global simulations show that the switch of underlying turbulence from ITG to TEM does not generally induce an intrinsic rotation reversal. A rotation reversal during an ITG $\rightarrow$ TEM transition also depends on other plasma conditions. Figure 9 demonstrates ITG $\rightarrow$ TEM induced intrinsic rotation reversal in weak magnetic shear regime (not in general!). The underlying dynamics is again associated with the sign change of finite $k_{\|}$ (right panel of Fig. 9) and the fluctuation-generated stress (middle panel) during ITG $\rightarrow$ TEM transition in weak magnetic shear.

In summary, a first-principles-based model for intrinsic rotation prediction has been developed. Turbulence-driven residual stress is shown to account for both the shape and magnitude of the observed intrinsic toroidal rotation profiles in a set of DIII-D ECH plasmas. The characteristic dependence of residual stress and intrinsic rotation profile structure on the multi-dimensional parametric space covering turbulence type, q-profile structure, collisionality and up-down asymmetry in magnetic geometry has been studied with the goal of developing physics understanding needed for rotation profile control and optimization. Interesting results obtained include intrinsic rotation reversal induced by ITG-TEM transition in flat-q profile regime and by change in q-profile from weak to normal shear. This work was supported by U.S. DOE Contract DE-AC02-09CH11466 and DE-FC02-04ER54698. DIII-D data shown in this paper can be obtained in digital format by following the links at https://fusion.gat.com/global/D3D_DMP. The GTS simulations were carried out on Edison at the National Energy Research Scientific Computing Center.

# References

[1] W. X. Wang *et al.*, Phys. Plasmas **13**, 092505 (2006).

[2] W. X. Wang *et al.*, Phys. Plasmas **17**, 072511 (2010).

[3] B. Scott and J. Smirnov, Phys. Plasmas 17 112302 (2010).

[4] P. H. Diamond *et al.*, Nucl. Fusion **49**, 045002 (2009).

[5] R. Dominguez and G. M. Staebler, Phys. Fluids, B **5**, 3876 (1993).

[6] O. D. Gurcan *et al.*, Phys. Plasmas **14**, 042306 (2007).

[7] W. X. Wang *et al.*, Phys. Rev. Lett. **102**, 035005 (2009).

[8] Y. Camenen *et. al.*, Phys. Plasmas **16**, 012503 (2009).

[9] O. D. Gurcan *et al.*, Phys. Plasmas **17**, 112309 (2010).

[10] Y. Camenen *et. al.*, Nucl. Fusion **51**, 073039 (2011).

[11] Z. X. Lu *et. al.*, Phys. Plasmas **22**, 055705 (2015).

[12] F. I. Parra *et. al.*, Phys. of Plasmas **18**, 062501 (2011).

[13] N. Mattor and P. H. Diamond, Phys. Fluids **31**, 1180 (1988).

[14] A. G. Peeters *et. al.*, Phys. of Plasmas **12**, 072515 (2005).

[15] P. H. Diamond *et al.*, Nucl. Fusion **53**, 104019 (2013).

[16] Z. X. Lu *et. al.*, Nucl. Fusion **55**, 093012 (2015).